Longitudinal optical and spin Hall conductivities of Rashba conducting strips coupled to ferromagnetic and antiferromagnetic layers

José A. Riera
Instituto de Física Rosario (CONICET) and Universidad Nacional de Rosario, Rosario, Argentina
(Received 28 October 2016; revised manuscript received 4 January 2017; published 30 January 2017)

A system composed of a conducting planar strip with Rashba spin-orbit coupling (RSOC), magnetically coupled to a layer of localized magnetic moments, at equilibrium, is studied within a microscopic Hamiltonian with numerical techniques at zero temperature in the clean limit. In particular, transport properties for the cases of ferromagnetic (FM) and antiferromagnetic (AFM) coupled layers are computed in linear response on strips of varying width. Some behaviors observed for these properties are consistent with the ones observed for the corresponding Rashba helical currents. The case of uncoupled Rashba strips is also studied for comparison. In the case of Rashba strips coupled to an AFM localized order, results for the longitudinal dc conductivity, for small strip widths, suggest the proximity to a metal-insulator transition. More interesting, in the proximity of this transition, and in general at intermediate values of the RSOC, a large spin Hall conductivity is observed that is two orders of magnitude larger than the one for the FM order for the same values of the RSOC and strip widths. There are clearly two different regimes for small and for large RSOC, which is also present in the behavior of Rashba helical currents. Different contributions to the optical and the spin Hall conductivities, according to a new classification of inter- or intraband origin proposed for planar strips in the clean limit, or coming from the hopping or spin-orbit terms of the Hamiltonian, are examined. Finally, the effects of different orientation of the coupled magnetic moments will be also studied.

DOI: 10.1103/PhysRevB.95.045146

I. INTRODUCTION

There is currently an increasing interest in studying and developing new systems and devices that could process information using the spin of the electron, which is the essence of the field of spintronics [1–4]. In particular, a considerable number of possibilities stem from the implementation of effective couplings derived from microscopic spin-orbit (SO) interactions, chief among them the Rashba spin-orbit coupling (RSOC), which appears in systems with structural inversion asymmetry [5–9].

It has been recently noticed [10–13] that a strong spin torque can be induced on ferromagnets (FM) coupled to a two-dimensional (2D) layer with Rashba SOC. This process was observed when an electrical current flows in the plane of a Co layer with asymmetric Pt and AlOx interfaces [13–15]. Even more recently, it has been discussed the possibility of an analogous relativistic SO torque appearing when an antiferromagnetic (AFM) layer is coupled to a conducting layer containing RSOC [16,17]. It was also suggested that this possibility could be realized in bulk Mn_2Au, which although is centrosymmetric, it can be divided into two sublattices that separately have broken inversion symmetry. This second possibility is referred to as a Néel SO torque (NSOT), to differentiate it from the previously mentioned FM SO torque (FSOT). In these two systems, the FM or AFM order in the magnetic layer is fixed due to a large enough exchange interaction among localized magnetic moments. Possible advantages of spintronic devices involving AFM layers, for example, their fast magnetic dynamics and the insensitivity to stray fields, are well-known [18,19]. Remarkably, it was recently found that the NSOT could drive an antiferromagnetic domain wall at velocities two orders of magnitude greater than the ones in ferromagnets [20,21].

Rashba SO coupling leads to the spin Hall effect [7,8], which manifests itself on finite width systems or strips, as spin accumulation at the strip edges [22–24]. Perhaps the most important quantity related to these effects is the spin Hall conductivity, which in clean 2D systems turned out to be a constant independent of the Rashba strength for a wide range of electron fillings [25]. Subsequent studies lead to the conclusion that the spin Hall conductivity vanishes in the presence of scattering [26]. This result led in turn to some controversial interpretation of experimental data. Most of this theoretical work has been performed on unbounded 2D systems and using a parabolic band, that is, with infinite bandwidth. Many shortcomings and peculiar results obtained for these systems have been stressed in the literature. Specifically, the above mentioned controversy concerning the spin Hall conductivity was settled down once the effect of parabolic bands was recognized, that is, the spin Hall conductivity is finite and in general proportional to the square of the Rashba SOC, as soon as the kinetic energy term departs from the parabolic form [27]. On the other hand, planar strips or wires, rather than unbounded 2D systems, and tight-binding bands with finite bandwidth, are in general more realistic, particularly for new materials or mechanisms which have been proposed for spintronic devices and where larger electron fillings may be involved, such as for example, those involving $LaAlO_3/SrTiO_3$ interfaces [28,29]. It should also be noticed that on planar strips, at equilibrium, using second quantization, which allows wave-functions to be finite at the edges, the presence of Rashba helical currents close to the strip edges have been reported [30].

Hence the purpose of the present work is to study the optical and spin Hall conductivities of conducting strips with a Rashba SOC in contact with a magnetized slab with FM or AFM orders. Although the above mentioned FSOT and NSOT occur in off-equilibrium systems, the study of an appropriate microscopic model Hamiltonian in second quantization at equilibrium, and within linear response, could shed some light on the behavior of systems in off-equilibrium regimes,

particularly for strips. Certainly, the simplified model here considered does not capture many details at the interfaces of the actual devices [15,17,29], but this simplicity is necessary to provide general insights that could help the search for new materials or devices. These microscopic insights on the various physical properties examined refer in the first place to the hopping or Rashba SO origin of the involved currents, and in second place, to a classification here proposed for the energy subbands or modes as a function of momentum that are characteristic of strips or wires. This classification of energy-momentum points, discussed in Sec. IV A, leads in turn to a classification of inter- and intraband transitions, which should not be confused with the ones used in theoretical studies for the unbound plane, in nonequilibrium regimes and in the presence of disorder (see for example, Ref. [41]).

For the sake of comparison, the case of isolated Rashba conducting strips, that is, not connected to a magnetic layer, will also be studied. It is also interesting to examine the Rashba helical currents, and to correlate their behavior is correlated with the one observed through the optical and spin Hall conductivities. These studies are performed assuming that the magnetic moments are always collinear. This assumption is realistic since the exchange interaction between moments in the coupled layer is typically very larger [21]. In the final Section, the effects of various possible orientations of the coupled magnetic order, for both the FM and AFM layers, will be examined, particularly for the AFM case when the magnetic moments are oriented along a direction that is parallel to the conducting plane, which is the situation considered in Ref. [17].

II. MODEL AND METHODS

The Hamiltonian here studied is $H = H_0 + H_{\rm int}$, where [17,31]

$$\begin{aligned} H_0 &= -t \sum_{\langle l,m\rangle,\sigma} (c^\dagger_{l\sigma} c_{m\sigma} + \text{H.c.}) + \lambda \sum_l [c^\dagger_{l+x\downarrow} c_{l\uparrow} \\ &\quad - c^\dagger_{l+x\uparrow} c_{l\downarrow} + i(c^\dagger_{l+y\downarrow} c_{l\uparrow} + c^\dagger_{l+y\uparrow} c_{l\downarrow}) + \text{H.c.}] \\ H_{\rm int} &= -J_{sd} \sum_l \mathbf{S}_l \cdot \hat{\mathbf{s}}_l + J \sum_{\langle l,m\rangle} \mathbf{S}_l \cdot \mathbf{S}_m, \end{aligned} \tag{1}$$

where l,m are sites on a square lattice, located on the $\{x,y\}$ plane, $\mathbf{S}_l$ are the localized magnetic moments, assumed classical, and $\hat{\mathbf{s}}_l$ are the spin of the conduction electrons (its operator nature is made explicit for later usage). The longitudinal (transversal) direction of the strip corresponds to the x axis (y axis). H_0 is the noninteracting part, which includes the hopping and RSOC terms with coupling constants t and λ, respectively. The RSOC term corresponds to an effective Rashba electric field along the z axis, i.e., perpendicular to the plane of the strip. Since both terms in H_0 contribute to the total kinetic energy, we choose the normalization $t^2 + \lambda^2 = 1$, whose square root will then be adopted as the unit of energy. With this normalization, the kinetic energy, and hence the total energy for fixed J, J_{sd}, turns out to be approximately constant as λ/t is varied [31]. Hence all the physical properties studied in the following will solely depend on the ratio λ/t, for given values of J, J_{sd}. The interacting part of the Hamiltonian contains a ferromagnetic coupling between conduction electrons and localized magnetic moments with strength J_{sd}, and an exchange interaction between magnetic moments with coupling J. Hamiltonian (1) is just a ferromagnetic Kondo lattice model with a Rashba SO coupling.

For the FM case, for most of the calculations, a value of $J_{sd} = 10$ will be adopted, which corresponds to the case of well-separated spin-up and spin-down conduction bands. For $J_{sd} = 5$, the bands are partially separated and in this case an AFM or staggered order along the y direction would be energetically favourable if the magnetic moments were allowed to rotate, for $J = 0$ [32]. For this reason the AFM order will be studied for $J_{sd} = 5$, although some results for $J_{sd} = 10$ will be also presented. In general, results do not qualitative change for this case in this range of J_{sd}. For the FM case, some results obtained by varying J_{sd} will be discussed in Sec. IV B though. Since FM and AFM orders are put by hand, the value of J is irrelevant since it only adds a constant to the total energy. The direction of the magnetic moments is adopted to be along the z axis. Since model (1) corresponds to a quantization axis along the z axis, it is expected that results will depend on the direction of the magnetic moments, and this issue will be examined in the final section.

Hamiltonian (1) will be studied on strips of length L and width W, with periodic (open) boundary conditions along the longitudinal (transversal) direction. $N = LW$ is the number of sites on the strip.

For classical localized magnetic moments, which is the assumption usually adopted in this context, the Hamiltonian becomes an extended tight-binding problem which is solved by numerical exact diagonalization for clusters with $2 \leqslant W \leqslant 64$ and $256 \leqslant L \leqslant 8000$. In all results presented below, finite size effects with respect to L are negligible. All results presented below correspond to quarter filling, $n = 0.5$.

The main quantities studied are the spin-conserving currents, $J_{\sigma,\hat{\mu}}, \sigma = \uparrow,\downarrow, \hat{\mu} = x,y$, defined as the expectation value of the operator:

$$\hat{j}_{\sigma,l,\hat{\mu}} = it(c^\dagger_{l+\hat{\mu},\sigma} c_{l,\sigma} - \text{H.c.}), \tag{2}$$

in units where the electron charge $e = 1$, and $\hbar = 1$, and the spin-flipping currents, $J_{\text{SO},\hat{\mu}}$, which are the expectation value of the operators:

$$\begin{aligned} \hat{j}_{\text{SO},l,\hat{x}} &= -i\lambda(c^\dagger_{l+x\downarrow} c_{l\uparrow} - c^\dagger_{l+x\uparrow} c_{l\downarrow} - \text{H.c.}), \\ \hat{j}_{\text{SO},l,\hat{y}} &= \lambda(c^\dagger_{l+y\downarrow} c_{l\uparrow} + c^\dagger_{l+y\uparrow} c_{l\downarrow} + \text{H.c.}). \end{aligned} \tag{3}$$

These expressions can be obtained in an standard way by introducing appropriate Peierls factors in the Hamiltonian (1) and taking the first derivative with respect to the magnetic flux. These currents also satisfy the charge conservation law, given generically by $\nabla \cdot \hat{\mathbf{j}} = -\partial n/\partial\tau$, where n is the occupation number operator and τ is the time, as long as $\partial n/\partial\tau = i[H_0,n]$, which will be further discussed below.

In equilibrium, due to translation invariance along x, all currents along x depend only on the chain position given by y. In all the cases analyzed below, in the absence of external electromagnetic sources, the SO currents along the strip direction are zero, except for the case of Rashba strips connected to a FM layer as it will be discussed in Sec. IV B. In all cases, vertical currents are also zero, except for the case of a constant orientation of the magnetic moments forming an

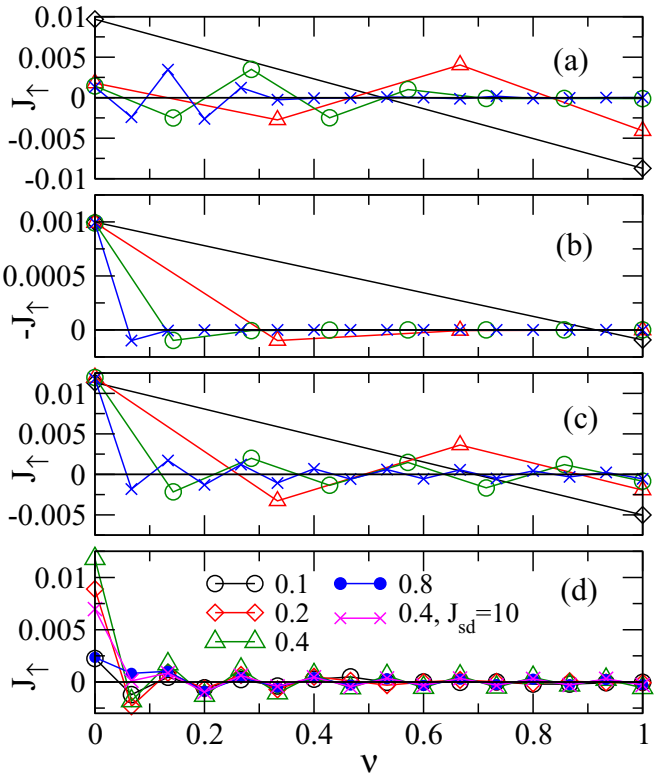

FIG. 1. Spin-up current on each chain as a function of the depth of the chain ($\nu = 0$, edge, $\nu = 1$, center chain), for $\lambda/t = 0.4$, (a) isolated Rashba conducting strip ($J_{sd} = 0$), (b) FM layer, $J_{sd} = 10$, and (c) AFM layer, $J_{sd} = 5$. Results correspond to strips with width $W = 4$ (diamonds), 8 (up triangles), 16 (circles), and 32 (crosses). In (d), Spin-up currents are shown for various values of λ/t indicated on the plot, AFM layer, $J_{sd} = 5$ (except the one corresponding to $J_{sd} = 10$), $W = 32$.

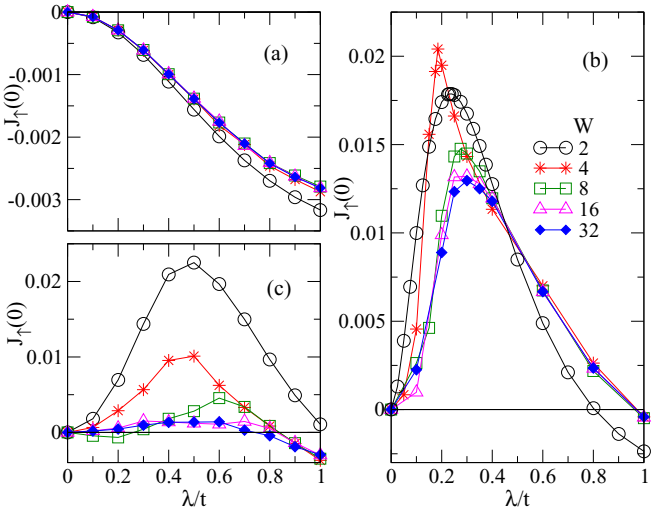

FIG. 2. Spin-up current on the edge chain as a function of λ/t, for various strip width W indicated on the plot, (a) fixed FM state $J_{sd} = 10$, (b) fixed AFM state $J_{sd} = 5$, and (c) isolated Rashba strip, $J_{sd} = 0$.

angle $\theta = \pi/3$ considered in Sec. V, where a more complex pattern appears. Certainly, the sum over the strip section of charge currents, as well as the sum over the strip section of spin currents, is always zero.

III. RASHBA HELICAL CURRENTS

The Rashba helical currents (RHCs), are counterpropagating spin-up and spin-down electron currents, that is of hopping or spin-conserving nature, at each link at the lattice [30], and they appear due to the RSOC acting on both x and y directions on the strip, in equilibrium and in the absence of any external electromagnetic field. It should be emphasized that they appear as a consequence of some boundary imposed on the system, or eventually in the presence of impurities [33]. Their existence can be inferred at an effective level [30] or by the structure of the RSOC [33,34]. Of course, the total current along the strip is zero. In the following we will compute RHCs, defined by the spin-up current along x, $J_\uparrow$, on each chain of closed strips of width W.

The RHCs on each chain as a function of its distance ν to the edge [$\nu = 0$, edge chain ($y = W$), $\nu = 1$, center chain ($y = W/2 + 1$)] are shown in Figs. 1(a)–1(c) for various strip widths, $\lambda/t = 0.4$, and different orderings of the magnetic layer. Figure 1(a) corresponds to conducting strips decoupled from the magnetic layer, that is $J_{sd} = 0$. This is the case previously studied, presenting characteristic sign oscillations with wave vector π, at $n = 0.5$, and mostly concentrated near the edges [30]. In Fig. 1(b), the conducting strip is coupled to a FM layer by a large value of $J_{sd} = 10$, corresponding to well-separated $s^z > 0$ and $s^z < 0$ bands, where $s^z = \langle \hat{s}^z \rangle_{sp}$, $\langle ... \rangle_{sp}$ meaning the average over a single-particle state. This is not a fully polarized system in the sense that for each band, $|s^z| < 1/2$. In this case, RHCs are only noticeable from zero at the strip edge, and effects of finite strip width are negligible. Sign oscillations are mostly absent. A very different behavior is observed for the case of an AFM spin background, as shown in Fig. 1(c). In this case, RHCs are also maximal near the edge. At the edge, $J_\uparrow(\nu = 0)$ is more than an order of magnitude larger than the one for the FM case, and it does not depend on the strip width. Besides, similarly to the decoupled system, they present sign oscillations as a function of ν. Notice also that the direction of $J_\uparrow(\nu = 0)$ is the same as the one for the pure Rashba strip and is opposite to the one of the FM coupled layer case.

The dependence of RHCs with λ/t for the AFM background, for $W = 32$ and $J_{sd} = 5$, is shown in Fig. 1(d). It is apparent that $J_\uparrow(\nu)$ grows with λ/t up to $\lambda/t \approx 0.4$, in the same way that it was predicted and observed for the case of isolated conducting strips [30], and then it starts to decrease for larger λ/t. By increasing J_{sd}, the RHCs decreases, as is illustrated for $\lambda/t = 0.4$ and $J_{sd} = 10$.

For a more systematic study, from now on only the RHCs on the outermost chains will be considered. In Fig. 2, the values of the RHC on the edge chain ($\nu = 0$) of strips with various widths are shown for different magnetic coupled layers as a function of λ/t. It can be seen in Fig. 2(a) that for the FM layer, the edge RHC in absolute value increases monotonically with λ/t in the range considered, with an initial shape which approximately follows the predicted quadratic

dependence for systems in the presence of a boundary [30]. At $\lambda/t \approx 0.5$, $J_\uparrow(0)$ experiences a change of curvature. This behavior is also virtually independent of W except for the smallest width considered, $W = 2$. In contrast, RHCs on the edge chains follow a nonmonotonic behavior for the AFM layer, as shown in Fig. 2(b). In this case, $J_\uparrow(0)$ presents a strong peak located at $0.2 \leqslant (\lambda/t)_{\rm peak} \leqslant 0.3$ for all W. The dependence with W is nonmonotonic for $\lambda/t \leqslant (\lambda/t)_{\rm peak}$, with the largest peak reached for $W = 4$. This peak becomes smoother and shifts to larger values of λ/t as W increases, although this variation with W seems to have converged for $W \approx 32$. It can be observed also that the the RHC curves in the region of $\lambda/t > (\lambda/t)_{\rm peak}$, fall onto a single curve, that is, they become independent of the strip width. Eventually $J_\uparrow(0)$ decreases to zero for $\lambda/t \approx 1$ for all W. Remarkably, for λ/t closer to the peak position, the RHCs for the AFM coupled layer are one order of magnitude larger than for the FM layer for all W, in agreement with the results shown in Figs. 1(b) and 1(c).

Results for the isolated conducting Rashba strip, $J_{sd} = 0$, are shown in Fig. 2(c) for comparison. $J_\uparrow(0)$ presents a broad maximum for $\lambda/t \approx 0.5$, that is larger than the peak of the AFM coupled layer for $W = 2$ but decreases rapidly by increasing W. Again, the dependence with W seems to be converged for $W \approx 32$. In all cases, the behavior of $W = 2$ seems somewhat different than for wider strips. This can be attributed to the fact that for $W = 2$ both chains are "outermost," while $W > 2$, the RHCs are spread over the strip section.

IV. TRANSPORT PROPERTIES

In this section, the main transport properties appearing as the response to some applied electromagnetic field, and that determine the suitability of Rashba strips coupled to magnetic layers for spintronic applications, that is, the optical conductivity and the spin Hall conductivity, are going to be studied. It is also important to examine if the behavior of the Rashba helical currents observed in the preceding section can be correlated with the behavior of these transport properties.

The optical conductivity is defined as the real part of the linear response to an electric field and can be written as [35]

$$\begin{aligned}\sigma(\omega) &= D\delta(\omega) + \sigma^{\rm reg}(\omega)\\ &= D\delta(\omega) + \frac{\pi}{N}\sum_{n\neq 0}\frac{|\langle\Psi_n|\hat{j}_x|\Psi_0\rangle|^2}{E_n - E_0}\delta(\omega - (E_n - E_0))\end{aligned} \tag{4}$$

where the paramagnetic current along the x direction is defined in terms of the currents defined in Eqs. (2) and (3) as

$$\begin{aligned}\hat{j}_x &= \hat{j}_{{\rm hop},x} + \hat{j}_{{\rm SO},x},\\ \hat{j}_{{\rm hop},x} &= \hat{j}_{\uparrow,x} + \hat{j}_{\downarrow,x},\\ \hat{j}_{\sigma,x} &= \sum_l \hat{j}_{\sigma,l,x}, \quad \sigma = \uparrow,\downarrow,\\ \hat{j}_{{\rm SO},x} &= \sum_l \hat{j}_{{\rm SO},l,x},\end{aligned} \tag{5}$$

The Drude weight D is calculated from the f-sum rule as

$$\frac{D}{2\pi} = -\frac{\langle H_{0,x}\rangle}{2N} - I_{\rm reg}, \tag{6}$$

where $-\langle H_{0,x}\rangle$ is the total kinetic energy of electrons along the x direction, and

$$I_{\rm reg} = \frac{1}{N}\sum_{n\neq 0}\frac{|\langle\Psi_n|\hat{j}_x|\Psi_0\rangle|^2}{E_n - E_0} \tag{7}$$

is the integral of the regular part of the optical conductivity. Notice that from Eq. (1), $\langle H_{0,x}\rangle = \langle H_{0,{\rm hop},x}\rangle + \langle H_{0,{\rm SO},x}\rangle$. In addition, taking into account the two contributions to the total current, given by Eq. (5), $I_{\rm reg}$ has a contribution from hopping currents, $|\langle\Psi_n|\hat{j}_{{\rm hop},x}|\Psi_0\rangle|^2$, another contribution from SO currents, $|\langle\Psi_n|\hat{j}_{{\rm SO},x}|\Psi_0\rangle|^2$, and the contribution from the cross terms, $2{\rm Re}\{\langle\Psi_n|\hat{j}_{{\rm hop},x}|\Psi_0\rangle\langle\Psi_0|\hat{j}_{{\rm SO},x}|\Psi_n\rangle\}$.

The spin Hall conductivity σ_{sH} is defined as the $\omega = 0$ limit of the spin-charge transversal response function given by the Kubo formula, at zero temperature [25,26]:

$$\sigma^{sc}_{xy}(\omega) = -i\frac{1}{\pi N}\sum_n\sum_m\frac{\langle\Psi_n|\hat{j}^s_y|\Psi_m\rangle\langle\Psi_m|\hat{j}_x|\Psi_n\rangle}{[(E_n - E_m)^2 - \omega^2]}, \tag{8}$$

where j^s_y is the spin current along the y direction. In the first sum, the summation is performed only over states with energies E_n larger than the Fermi energy E_F, and in the second sum only over states with energies $E_m < E_F$.

The definition of the spin current in Rashba systems has been extensively discussed [36–38] and perhaps this issue is still unresolved but a physically reasonable and well-defined expression from the operatorial point of view is the one that is derived from the spin conservation equation in the absence of external torques: $\nabla\cdot\hat{\mathbf{j}}^{\mathbf{s}} + \partial\hat{S}^z/\partial\tau = 0$ (τ is the time). From this expression, the spin current along the transversal direction can be computed as

$$\hat{j}^s_{y,l} = -i\big[H_{y,l},\hat{s}^z_l\big], \tag{9}$$

where $H_{y,l}$ contains the terms in Eq. (1) involving sites l and $l + y$. This expression is a stronger form of the spin conservation equation written above. Since on-site terms of the Hamiltonian could not lead to quantities considered as "currents," then $[H_{y,l},\hat{s}^z_l]$ should be replaced by $[H_{0,y,l},\hat{s}^z_l]$ [39], and the following expressions for $\hat{j}^s_y$ are obtained:

$$\begin{aligned}\hat{j}^s_y &= \hat{j}^s_{{\rm hop},y} + \hat{j}^s_{{\rm SO},y},\\ \hat{j}^s_{{\rm hop},y} &= \frac{1}{2}(\hat{j}_{\uparrow,y} - \hat{j}_{\downarrow,y}),\\ \hat{j}^s_{{\rm SO},y} &= -\frac{\lambda}{2}\sum_l(c^\dagger_{l+y\downarrow}c_{l\uparrow} - c^\dagger_{l+y\uparrow}c_{l\downarrow} + {\rm H.c.}).\end{aligned} \tag{10}$$

This expression for the spin currents, containing two terms, one from the hopping and another from the Rashba SO terms of the Hamiltonian (1), is the second quantized equivalent form of the one considered in previous works formulated in first quantization and using a parabolic kinetic energy [25]. Clearly, from Eqs. (5) and (10), there will be in principle four independent contributions to σ_{sH} which are computed and studied separately.

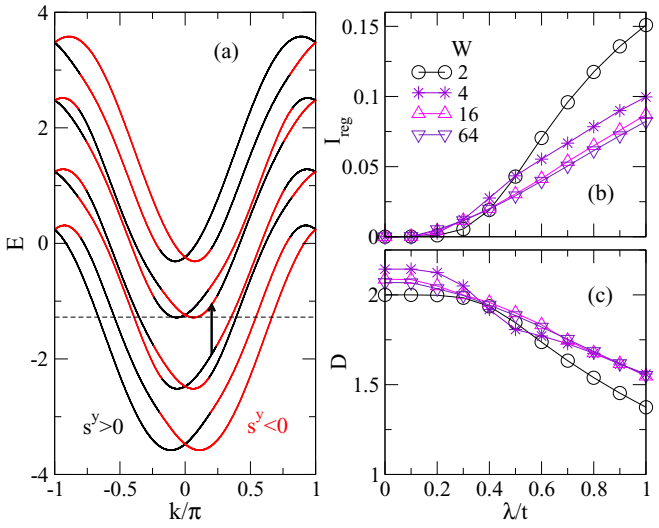

FIG. 3. (a) Energy bands with $s^y > 0$ (black) or $s^y < 0$ (red), $W = 4$, $\lambda/t = 0.4$. k is the momentum along the longitudinal direction. The dashed line indicates the chemical potential. (b) Integral of the regular part of the optical conductivity, and (c) Drude weight, as a function of λ/t for various strip widths W. Isolated, $J_{sd} = 0$, $L = 2000$ Rashba strips.

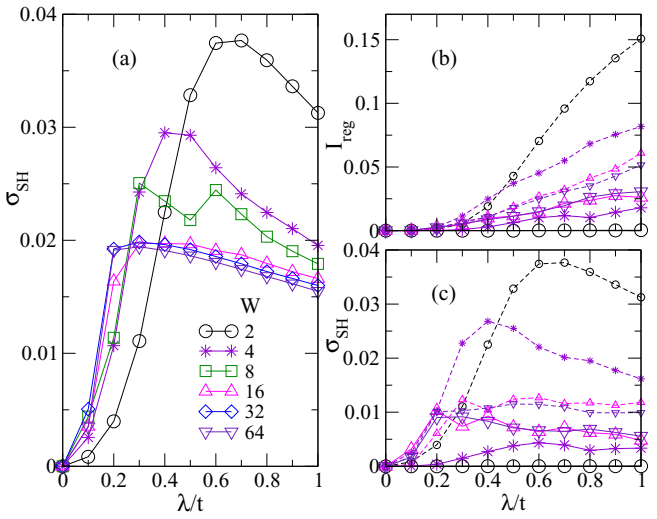

FIG. 4. (a) Total spin Hall conductivity, (b) inter- (dashed lines) and intra- (full lines) band contributions to I_{reg}, and (c) inter- and intraband contributions to the spin Hall conductivity, as a function of λ/t for various strip widths W indicated on the plot. Isolated, $J_{sd} = 0$, $L = 2000$ Rashba strips.

A. Isolated Rashba strips

Let us start by examining isolated conducting Rashba strips ($J_{sd} = 0$). In Fig. 3(a), the single-particle bands, $E(k)$, where k is the momentum along x, is shown for $W = 4, \lambda/t = 0.4$. The number of bands is equal to the number of coupled chains or "modes." The RSOC splits each band into two subbands with different sign of $s^y = \langle \hat{s}^y \rangle_{sp}$ [9,40]. Note that for the strips here considered, as a difference with the case of the unbounded 2D system [40], s^y is not a good quantum number. Also, due to the breaking of spatial rotational invariance, only the value of s^y, related to the momentum along the strip axis, is needed to label $\{k, E(k)\}$ points. Note also that on each of the subbands, the sign of s^y changes.

In the following, the expressions "interband transitions" or "intraband transitions" will refer to transitions between states with opposite or the same sign of s^y respectively. This is a natural extension of the concept of intraband and interband processes used for the infinite plane [25,26] to finite-width strips, in the clean limit, and it also avoids the problem of the presence of the multiple subbands appearing with strips. More importantly, with this definition, interband transitions would be detectable by optical experiments [40]. In the literature, in systems in a nonequilibrium regime, and in the presence of impurities, other definitions of inter- and intraband transitions have been used [41].

A typical interband transition contributing to the lowest peak in $\sigma(\omega)$ is shown in Fig. 3(a). The inter- and intraband contributions to $I_{\rm reg}$ and σ_{sH} will be discussed below.

Clearly, the behavior of $E(k)$ is metallic for all electron fillings, and for $n = 0.5$, the chemical potential is located close to a maximum of the density of states or van-Hove singularity. In Fig. 3(b), results for the integral of the regular part of the optical conductivity, $I_{\rm reg}$, are shown as a function of λ/t for various strip widths indicated on the plot. The main result is that $I_{\rm reg}$ is due entirely to the SO currents defined in Eq. (5). The Drude weight D is shown in Fig. 3(c). Both quantities present a nonmonotonic behavior as a function of W, and cusps around $\lambda/t \approx 0.4$–0.5 can be noticed for $W = 2$ and 4, which is consistent with the behavior of the RHCs shown in Fig. 2(c),

In Fig. 4(a), the spin Hall conductivity is shown for various strip widths as a function of λ/t. In this case, σ_{sH} turns out to be entirely due to the $\langle \hat{j}^{s}_{{\rm SO},x} \hat{j}^{s}_{{\rm hop},y} \rangle$ (for short) contribution. σ_{SH} has a strong dependence with W, with a maximum shifting to lower vales of λ/t as W increases, although it seems that it is converging for $W = 64$. For the largest widths considered, $W = 32$ and 64, the spin Hall conductivity presents a flat region reminiscent of the constant value predicted in Ref. [25], although this prediction was obtained for the infinite 2D system with a parabolic dispersion. Notice also that with the normalization here adopted for the parameters t and λ, presumably additional factors should have to be taken into account to compare the present results with those of Ref. [25]. For the widest strips, the presence of a cusp separating two different regimes is clearly visible, and in this case, the cusp is not correlated with the peaks observed in the RHCs curves.

In Figs. 4(b) and 4(c), the inter- and intraband contributions to the $I_{\rm reg}$ and to σ_{sH} are shown. In both cases, it is remarkable that for $W = 2$ both quantities are purely of inter-band origin, and that as W increases the inter- and intraband processes tend to equally contribute to those quantities.

B. Coupled FM layer

Let us now consider the more interesting case of a fixed FM layer coupled to the conducting strip by a ferromagnetic exchange $J_{sd} = 10$. In Fig. 5(a), the dispersion relation for $W = 4$ and $\lambda/t = 0.4$ is depicted. $E(k)$ points have been labeled by the sign of s^y. The negative energy bands have also $s^z > 0$ and are separated from the positive energy bands

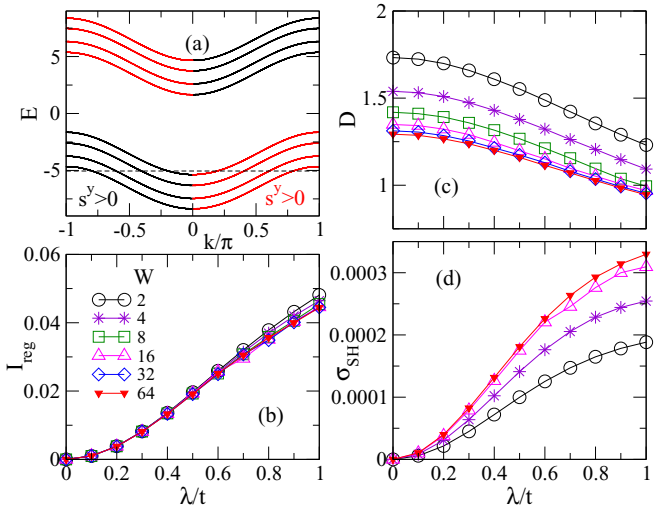

FIG. 5. (a) Band structure for $W = 4$, $\lambda/t = 0.4$. (b) $I_{\rm reg}$, (c) Drude weight, and (d) spin Hall conductivity, as a function of λ/t for various strip widths W, for a fixed FM layer, $J_{sd} = 10$.

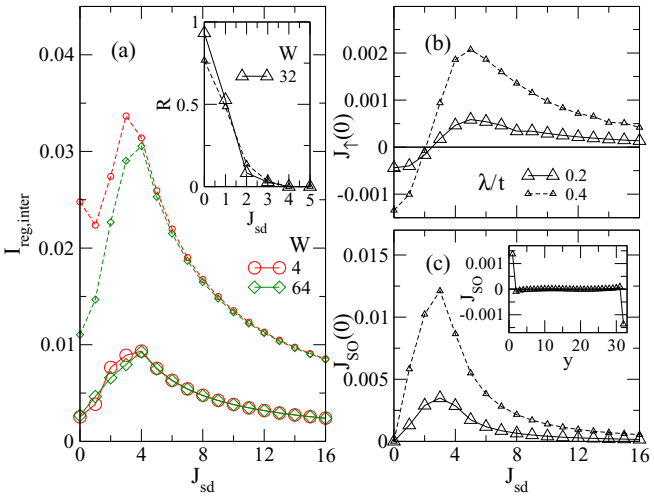

FIG. 6. (a) Interband contribution to $I_{\rm reg}$ for $W = 4$ (circles) and $W = 64$ (diamonds), $\lambda/t = 0.2$ and 0.4, as a function of J_{sd}. The inset in (a) shows the ratio R between the intraband and the interband contributions to $I_{\rm reg}$, $W = 32$. (b) Rashba helical currents, and (c) SO currents on the edge chain, as a function of J_{sd}, $W = 32$. The inset in (c) shows $J_{\rm SO}$ on each chain of the $W = 32$ strip, $\lambda/t = 0.4$. Coupled FM layer. In all plots, results for $\lambda/t = 0.2$ are shown with full lines, while those for $\lambda/t = 0.4$, with dashed lines.

with $s^z < 0$ due to the finite value $J_{sd} = 10$. The optical conductivity $\sigma(\omega)$ presents a single peak at $\omega \approx 10$ and it is originated in interband transitions, as can be inferred from the s^y character of the bands. This will be further discussed below.

In Fig. 5(b), $I_{\rm reg}$ is shown as a function of λ/t for various strip widths W. Again, this quantity is due entirely to the SO currents. and it is almost independent of W. The Drude weight, shown in Fig. 5(c), decreases as W increases due to a reduction of the kinetic energy along the longitudinal direction. The vanishing of intraband contributions to the longitudinal conductivity is consistent with recent results obtained for an infinite isotropic two-dimensional system [42].

The spin Hall conductivity, shown in Fig. 5(d), also presents a rather monotonic behavior as a function of λ/t. This monotonic behavior in both D and σ_{sH} is also similar to the one observed for the RHCs in Fig. 2(a), although there is no direct causality between these features. The spin Hall conductivity is also entirely due to the $\langle \hat{j}^{s}_{{\rm SO},x}\, \hat{j}^{s}_{{\rm hop},y}\rangle$ contribution, and it almost entirely involves interband processes, except for marginal intraband contributions. Notice that in the present case, as well as in the previous case of isolated Rashba strips, σ_{sH} follows an approximate quadratic dependence with the Rashba SOC, particularly for small λ/t, consistently with the prediction of Ref. [27].

Taking into account the different behaviors observed for the isolated Rashba strip, $J_{sd} = 0$, and the strip coupled to a FM layer with $J_{sd} = 10$, it is important and interesting to see the evolution of the various properties examined so far as J_{sd} is varied to zero to a large value. In principle, the behavior for the FM layer is not extrapolatable to $J_{sd} = 0$ due to the condition of well-separated bands, as shown in Fig. 5(a). The results of this study are shown in Fig. 6, and, as expected, it becomes apparent that this evolution with J_{sd} is nonmonotonous. It is clear that there is a regime of large J_{sd}, where the s^z up and down bands are well separated, and a regime of small J_{sd}, where these bands are partially overlapped. The crossover between both regimes takes place at $J_{sd} \approx 4$. In the region of large J_{sd}, $I_{\rm reg}$, as mentioned above is purely of interband origin and, as it can be observed in Fig. 6(a), this contribution decays approximately as J_{sd}^{-1}, as J_{sd} increases, for all values of W and λ/t considered. On the other hand, $I_{\rm reg,inter}$ decreases as J_{sd} is decreased from $J_{sd} \approx 4$, and at the same time, as it can be observed in the inset, the intraband contribution starts to grow until it becomes of the same order as the interband one at $J_{sd} = 0$.

The same behavior change can be observed in other quantities. For example in Fig. 6(b), it is shown that the RHC smoothly decreases in the large J_{sd} region as J_{sd} is increased, and it also decreases as J_{sd} is decreased when J_{sd} varies from $J_{sd} \approx 4$ towards zero, and it even change sign in this interval. It is also instructive to notice that for Rashba strips coupled to a FM layer, not only Rashba helical currents, which are currents of the hopping type, are present as in all systems considered in the present work, but also currents of the spin-flipping type, $J_{\rm SO}(y)$, along x, defined in Eq. (3), have a finite average on each chain. One could speculate that these currents appear for the FM coupled layer because the Rashba SO naturally tends to reduce the FM order, so the external fixing of a FM order leads to these currents to counteract that Rashba effect. In fact, if the orientation of the magnetic moments or the sign of J_{sd} are changed, then these helical currents of the SO type change their direction. The distribution of these SO currents over the strip section, shown in the inset of Fig. 6(c) is such that its net value is zero, as it should be in equilibrium. Again, as it can be seen in Fig. 6(c), two different behaviors of $J_{\rm SO}(0)$ can be noticed for J_{sd} greater or smaller than $\approx$4. Of course, consistently with the previous results, these spin-flipping currents have vanishing expectation value for $J_{sd} = 0$.

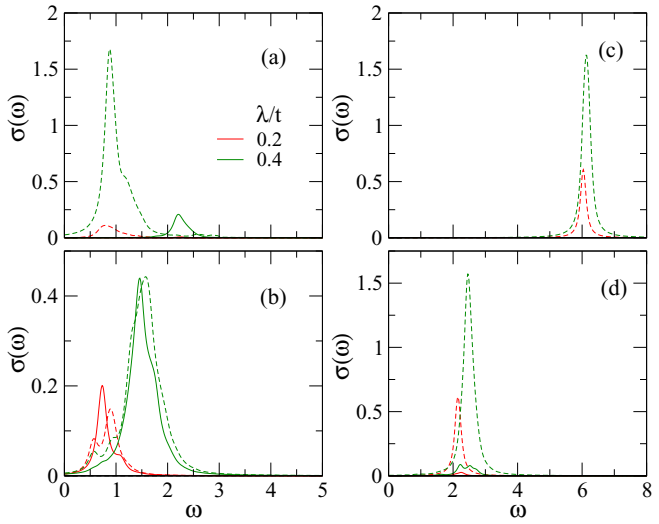

FIG. 7. Optical conductivity as a function of the frequency for isolated Rashba strips with (a) $W = 4$, (b) $W = 32$, and for Rashba strips coupled to a FM layer, $W = 16$, for (c) $J_{sd} = 6$, (d) $J_{sd} = 2$. Values of λ/t are indicated on the plot. In all plots, the interband (intraband) contribution is shown with dashed (full) lines, and $\sigma(\omega)$ has been multiplied by 10^3.

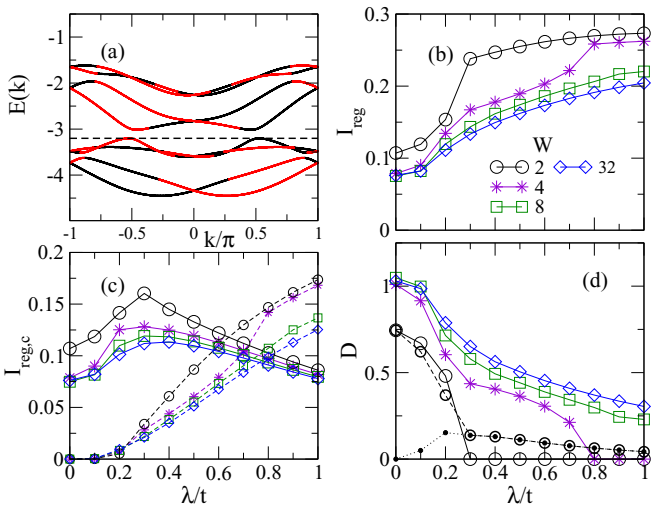

FIG. 8. (a) Lower half of the band structure, $s^y > 0$ (black) or $s^y < 0$ (red), $W = 4$, $\lambda/t = 0.4$. (b) $I_{\rm reg}$, and (c) contributions to $I_{\rm reg}$ from hopping (solid lines) and SO (dashed lines) currents, (d) Drude weight, as a function of λ/t, for coupled AFM layer, $J_{sd} = 5$. Results for $256 \times W$ strips with symbols for various W indicated on the plot. In (d), contributions to D from hopping (dashed line) and SO (dotted line) currents for $W = 2$ are also included.

To end this subsection, it is instructive to examine the frequency dependence of the optical conductivity for some typical cases. In Fig. 7(a), $\sigma(\omega)$ is shown for the isolated Rashba strip for $W = 4$, $\lambda/t = 0.2$ and 0.4. In this and related plots, a Lorentzian broadening $\epsilon = 0.01$ was adopted. For the $W = 4$ strip, consistently with the results shown in Fig. 4, for $\lambda/t = 0.2$, $\sigma(\omega)$ is almost entirely due to interband transitions, while for $\lambda/t = 0.4$, there is a small contribution from intraband transitions occurring at higher frequencies. On the other hand, for a wider strip, $W = 32$, Fig. 7(b), the inter- and intra-band contributions are approximately equal, and they are originated in transitions located at roughly the same frequencies. As noticed above regarding to Fig. 4, the optical conductivity for isolated strips, as well as for Rashba strips coupled to FM layers, are entirely due to SO currents, hence its intensity is always larger for larger λ/t. For the case of Rashba strips coupled to FM layers, in the regime of well-separated bands, or large J_{sd} region, the optical conductivity is purely of interband nature and it presents a single peak located at $\omega \approx |J_{sd}|$ for any value of λ/t. This case is shown in Fig. 7(c) for $J_{sd} = 6$, and $W = 16$, although in this region results are mostly independent of W. In the low J_{sd} region, when the bands start to overlap, as it can be seen in Fig. 7(d) for $J_{sd} = 2$, $W = 16$, the position of the largest peak starts to be shifted to to higher frequencies as λ/t increases, and, more importantly, an intraband contribution starts to grow. As discussed above, in this small J_{sd} region, one could expect a monotonous evolution from the behavior shown in Fig. 7(d) to the one in Fig. 7(b) as J_{sd} is reduced to zero.

C. Coupled AFM layer

Let us finally examine the most important case which is the one of a Rashba conducting strip coupled to an AFM layer. Figure 8(a) shows the lowest half energy bands of the $W = 4$ strip, $\lambda/t = 0.4$, where again $E(k)$ points have been labelled according to the sign of s^y. There is another set of energy bands symmetrically located with respect to $E = 0$. The two set of bands are separated in energy due to the finite $J_{sd} = 5$ value. A remarkable difference with respect to the two previous cases, is that the coupling to a AFM layer introduces small gaps whose sizes decreases with W and increases with J_{sd}. For $J_{sd} = 5$, the gap is present for $W \leqslant 8$, and disappears for $W \geqslant 16$. For $W \leqslant 8$ and $n = 0.5$, the Fermi level is just at the top of the energy branch below the gap, and hence close to a high density of states.

Figure 8(b) shows $I_{\rm reg}$ for various strip widths W, and Fig. 8(d) the corresponding results for the Drude weight. For the smallest strip widths, $W = 2,4$ there is a cusp at $\lambda/t \approx 0.3$, and $\lambda/t \approx 0.8$, that coincides with the value at which the respective Drude weights vanish. Notice that for widths $W > 2$, there is also a curvature change near $\lambda/t = 0.2$. It seems then that the decaying of the RHCs after their peak, shown in Fig. 2(b), may be correlated with the onset, for $W = 2$, or the proximity to a metal-insulator transition for $W > 2$. It is also interesting to note that the vanishing of the Drude weight for $W = 2,4$ is due to equal and opposite contributions from spin-conserving and spin- flipping currents, as shown in Fig. 8(d) for $W = 2$.

As expected from the complex pattern of $E(k)$ points with positive and negative values of s^y, and as expected from the already discussed case of free Rashba strips ($J_{sd} = 0$), $I_{\rm reg}$ will have contributions from both inter- and intraband processes. More interesting, and perhaps more physically appealing, $I_{\rm reg}$ has now contributions from both the SO (spin-flipping) and the hopping (spin-conserving) currents, as shown in Fig. 8(b). As expected, the contribution from $\hat{j}_{{\rm hop},x}$ ($\hat{j}_{{\rm SO},x}$) dominates at small (large) λ/t, Contributions from the mixed term are marginal.

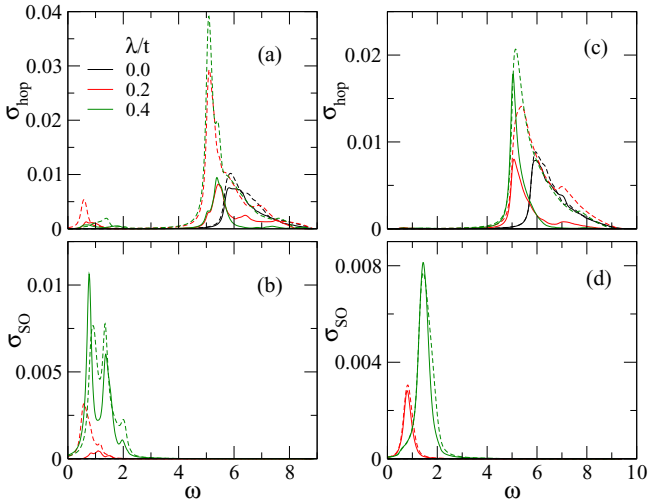

FIG. 9. Optical conductivity as a function of the frequency for Rashba strips coupled to AFM layers, $J_{sd} = 5$ with (a), (b) $W = 4$, and (c), (d) $W = 32$. The inter- and intraband contributions to the part of $\sigma(\omega)$ due solely to hopping currents are shown in (a) and (c), while the ones to $\sigma(\omega)$ due solely to the SO currents, in (b) and (d). Values of λ/t are indicated on the plot. In all plots, the interband (intraband) contribution is shown with dashed (full) lines.

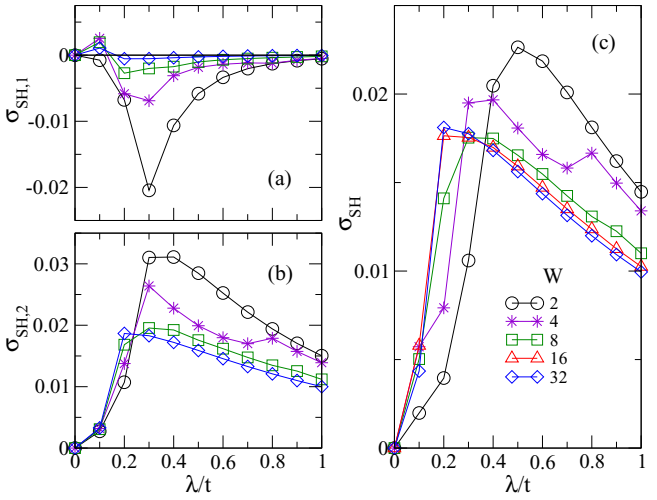

FIG. 10. (a) $\sigma_{sH,1}$ and (b) $\sigma_{sH,2}$ contributions to the spin Hall conductivity (see text), and (c) total spin Hall conductivity, as a function of λ/t, for coupled AFM layer, $J_{sd} = 5$, with symbols for various W indicated on the plot.

To understand the previous results for the optical conductivity, let us now show the frequency dependence of its various contributions. Figures 9(a) and 9(c) shows inter- and intraband contributions to the part of $\sigma(\omega)$ due solely to hopping currents, $\sigma_{\rm hop}(\omega)$, for $W = 4$ and 32, respectively, while Figs. 9(b) and 9(d), shows inter- and intraband contributions to the purely SO term, $\sigma_{\rm SO}(\omega)$, for $W = 4$ and 32, respectively. In the first place, consistently with the behavior shown in Fig. 8(c), the intensity of the largest peaks in $\sigma_{\rm hop}$ is larger than the ones in $\sigma_{\rm SO}$. Second, $\sigma_{\rm hop}$ is mostly of interband transitions, while $\sigma_{\rm SO}$ has contributions from both inter- and intraband transitions, and these contributions become approximately equal particularly as W and λ/t increase, similarly to what happens for isolated Rashba strips. It is quite apparent also that $\sigma_{\rm hop}$, which is absent in the cases of isolated Rashba strips and strips coupled to a FM layer shown in Fig. 7, presents the strongest peak located at $\omega \approx J_{sd}$, while $\sigma_{\rm SO}$ has its strongest peaks at low frequencies, and this behavior is again similar to the one observed for J_{sd}.

Perhaps the most important and interesting results of the present effort are the ones for the spin Hall conductivity. For the same reasons mentioned above, the spin Hall conductivity will also have contributions from both inter- and intraband processes. However, what may be more interesting, is the fact that σ_{sH} has contributions from both $\langle \hat{j}_{{\rm hop},x} \hat{j}^s_{{\rm hop},y} \rangle$ and $\langle \hat{j}_{{\rm SO},x} \hat{j}^s_{{\rm hop},y} \rangle$ terms. Contributions from the former lead to the term $\sigma_{sH,1}$, while contributions from the latter, to the term $\sigma_{sH,2}$. Results for $\sigma_{sH,1}$ and $\sigma_{sH,2}$ are shown in Figs. 10(a) and 10(b), respectively. The first conclusion is that both contributions have opposite signs, except for $\lambda/t \leqslant 1$, where both contributions are negative. It is also apparent that $\sigma_{sH,1}$ is suppressed faster with W. The total σ_{sH}, shown in Fig. 10(c) is hence dominated by the $\langle \hat{j}_{{\rm SO},x} \hat{j}^s_{{\rm hop},y} \rangle$ terms. The discontinuous behavior above discussed is also noticeable in Figs. 10(a) and 10(b), where a clear change of behavior can be seen in $0.2 \leqslant \lambda/t \leqslant 0.3$, that is coincidentally with the peak in the RHCs shown in Fig. 2(b).

The resulting behavior of σ_{sH}, shown in Fig. 10(c) is strikingly different to the one for FM coupled layers. While for the FM layer, as shown in Fig. 5(c), σ_{sH} increases with both λ/t and W, for the AFM case, σ_{sH} reaches a maximum that decreases with W, and this maximum is located at a value of λ/t that also decreases with W. The overall behavior of σ_{sH} is also similar to the one already reported for isolated Rashba strips [Fig. 4(a)], including their magnitude.

Last but not least, it is remarkable that the maximum value of σ_{sH} in the AFM background is more than two orders of magnitude larger than the one for the FM case for the same W and at the same value of λ/t, and this difference is even larger for narrower strip widths. The discussion of the interband or intraband character of the transitions leading to σ_{sH} are deferred to the next section.

V. OTHER ORIENTATIONS OF THE COUPLED MAGNETIC MOMENTS

Let us assume that the magnetic moments of the coupled layer can have an arbitrary but uniform orientation, forming an angle θ with respect to the z axis and an azimuthal angle φ with the x axis. Of course, in the absence of a Rashba SO coupling, the system is independent of θ, φ but for any nonzero λ, the physical properties will depend on the global orientation of the magnetic moments. Actually, by minimizing the ground-state energy of Hamiltonian (1), it turns out that the lowest energy state with uniform orientation of the magnetic moments, for the FM case, corresponds to $\theta = \pi/2$, $\varphi = 0$, that is, pointing along the x axis, in the regime of large J_{sd}, due to essentially a reduction of the J_{sd} exchange energy. The value of J is irrelevant since for uniform orientation of magnetic moments it would contribute to a constant independent of λ.

Alternatively, the magnetic moment orientation may be fixed by the structure of the materials involved in a given

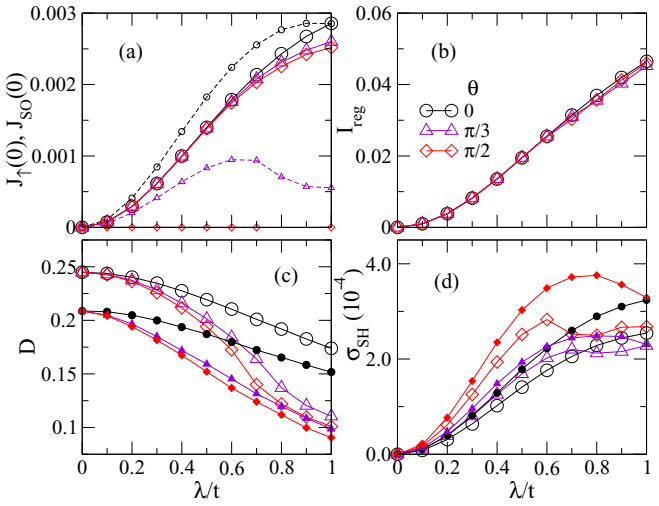

FIG. 11. (a) Rashba helical current at the edge, both of hopping (full lines) and SO (dashed lines) character, (b) integral of the regular part of the optical conductivity, (c) Drude weight, and (d) spin Hall conductivity, as a function of λ/t, for coupled FM layer, $J_{sd} = 10$, $W = 4$, and various orientations of the magnetic moments, θ indicated on the figure ($\varphi = 0$). In (c) and (d) results for $W = 32$ (full symbols) have been included.

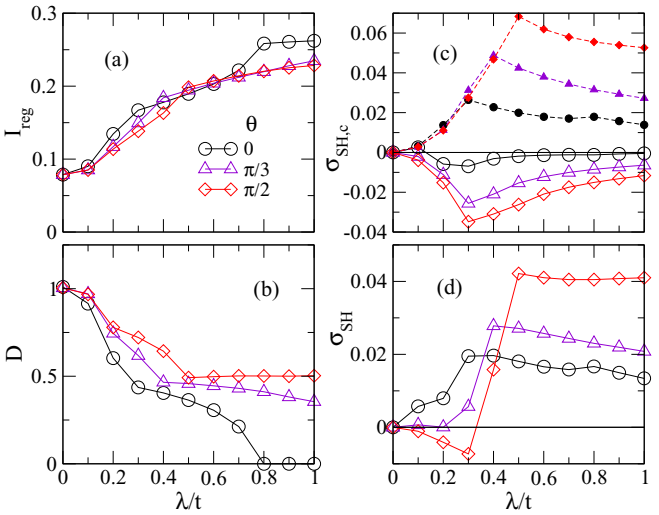

FIG. 12. (a) Integral of the regular part of the optical conductivity, (b) Drude weight, (c) $\sigma_{sH,1}$ (full lines) and $\sigma_{sH,2}$ (dashed lines) contributions to the spin Hall conductivity (see text), and (d) total spin Hall conductivity, as a function of λ/t, for coupled AFM layer, $J_{sd} = 5$, $W = 4$, and various orientations of the magnetic moments, θ, indicated on the figure. The azimuthal angle $\varphi = 0$.

device, so it is interesting to examine the dependence of transport properties with different orientations. Resuming the comment written after Eq. (9), notice that now due to the x component of the magnetic moments, both $\hat{s}^z$ and the occupation number operators, n_σ, do not commute with $H_{\rm int}$. However, the resulting contributions from these commutators are local, fieldlike operators, no currentlike ones. Hence, in the following, the previous expressions for charge and spin currents, given by Eq. (5) and Eq. (10), respectively, will be used to compute the optical and spin Hall conductivities.

In the following, two different global orientations of the magnetic moments, $\theta = \pi/3$ and $\pi/2$, with $\varphi = 0$, will be analyzed. Results for these two global orientations of the magnetic moments for the FM layer, $J_{sd} = 10$, are shown in Fig. 11, together with previous results for $\theta = \varphi = 0$ that are included for comparison. Most of these results were obtained for $W = 4$ but are qualitatively independent of the width, as it can be seen in Figs. 11(c) and 11(d), where the corresponding results for $W = 32$ were added. Figure 11(a) shows that the RHCs of hopping origin at the strip's edge, $J_\uparrow(0)$, only slightly decrease as θ increases from 0 to $\pi/2$, but the RHCs of SO origin, which are nonzero for the FM layer as discussed before, are strongly suppressed as θ is increased from zero, and vanish for $\theta = \pi/2$, that is when the magnetization is parallel to the strip plane. This is consistent with the previous comment after Fig. 6 about that the RHC-SO reverse their direction when the magnetic moments are inverted.

$I_{\rm reg}$, shown in Fig. 11(b), remains virtually unchanged when θ changes from 0 to $\pi/2$. Its SO origin, discussed in Sec. IV B, is also not modified by θ. There is a slight increase in the intraband contribution to $I_{\rm reg}$, but it still is much smaller than the interband one. Hence, mainly due to a reduction in the kinetic energy, it can be seen in Fig. 11(c), that the Drude weight is homogeneously suppressed by increasing θ. It is also interesting to notice the enhancement of the spin Hall conductivity for $\lambda/t \lesssim 0.7$ for $W = 4$ ($\lambda/t \lesssim 0.7$ for $W = 32$) as θ is increased from 0 to $\pi/2$, as it can be observed in Fig. 11(d). This enhancement occurs even though the $\langle \hat{j}_{{\rm SO},x} \hat{j}^s_{{\rm hop},y} \rangle$ origin of σ_{sH}, as well as its purely interband character, are not modified by θ.

Let us now consider the also interesting case of the AFM coupled layer. In this case, the direction of the magnetic moments is uniformly tilted with the constraint that magnetic moments on nearest-neighbor sites are kept antiparallel, that is, maintaining the AFM order. In this case, as a difference with the FM layer, if the antiparallel magnetic moments are freely rotated, the minimum of the total energy of the Hamiltonian would correspond to $\theta = \varphi = 0$, that is, they would point along the z axis.

Results for these two global orientations of the magnetic moments, for the $W = 4$ strip, $J_{sd} = 5$, are shown in Fig. 12, together with previous results for $\theta = \varphi = 0$ which are included for comparison. Figure 12(a) shows that $I_{\rm reg}$ does not depend significantly on θ. On the other hand, the Drude weight systematically increases with θ, particularly for $\lambda/t > 0.5$, as shown in Fig. 12(b), and this behavior can be attributed to the closing of the gaps shown in Fig. 8(a). However, even for $\theta = \pi/2$, a change in the curvature can still be clearly observed. The total spin Hall conductivity is shown in Fig. 12(d). At small values of the RSOC, σ_{sH} decreases with θ, while for larger values of the RSOC, it increases with θ. It is remarkable that for small values of λ/t, σ_{sH} has an opposite signs for $\theta = 0$ and $\theta = \pi/2$. This behavior could be traced to the behavior of the two nonzero contributions to σ_{sH}, shown in Fig. 12(c). For small λ/t, the $\sigma_{sH,1}$ contribution, due to the $\langle \hat{j}_{{\rm hop},x} \hat{j}^s_{{\rm hop},y} \rangle$ terms, grows rapidly with θ, while $\sigma_{sH,2}$, due to the $\langle \hat{j}_{{\rm SO},x} \hat{j}^s_{{\rm hop},y} \rangle$ terms, is virtually independent of θ. For large λ/t, $\sigma_{sH,2}$ grows in absolute value more rapidly than $\sigma_{sH,1}$, thus leading to the observed change in the behavior of the total σ_{sH}.

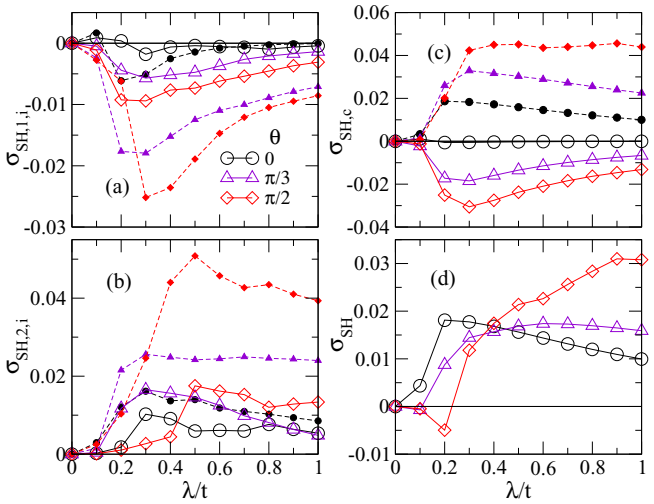

FIG. 13. Intra- (full lines) and inter-band (dashed lines) contributions to (a) $\sigma_{sH,1}$ and (b) $\sigma_{sH,2}$ (see text) as a function of λ/t, for $W = 4$, and various orientations of the magnetic moments, θ, indicated on the plot, $\varphi = 0$. (c) $\sigma_{sH,1}$ (full lines) and $\sigma_{sH,2}$ (dashed lines) contributions to the spin Hall conductivity, and (d) total spin Hall conductivity, as a function of λ/t, $W = 32$. Coupled AFM layer, $J_{sd} = 5$.

The inter- or intraband character of the transitions leading to σ_{sH} is shown in Fig. 13. Results depicted in Fig. 13(a), correspond to the inter- and intraband contributions to $\sigma_{sH,1}$ [shown with full lines in Fig. 12(c)], while the ones in Fig. 13(b), are for $\sigma_{sH,2}$ [shown with dashed lines in Fig. 12(c)]. In both cases, for virtually all values of λ/t, and for the three values of θ considered, the interband transitions are clearly dominant, but both inter- and intra-band contributions increase with θ. The previous results, as well as those of Fig. 12, correspond to the $W = 4$ strip. In Fig. 13(c), the two contributions $\sigma_{sH,1}$ and $\sigma_{sH,2}$, are shown for the $W = 32$ strip. As in Fig. 12(c), there is an increasing contribution from $\langle \hat{j}_{\mathrm{hop},x} \hat{j}^s_{\mathrm{hop},y} \rangle$ transitions, with an opposite sign to the $\langle \hat{j}_{\mathrm{SO},x} \hat{j}^s_{\mathrm{hop},y} \rangle$, which in absolute value are in all cases dominant. The total σ_{sH} for $W = 32$ is shown in Fig. 13(d), and similar behaviors as those previously pointed out for $W = 4$ are also present, particularly the sign change for small λ/t as θ increases from 0 to $\pi/2$.

If individual magnetic moments are allowed to rotate in order to minimize the ground state energy of Hamiltonian (1), it is found that the AFM order is unstable towards an AFM spiral, for $J \lessapprox 0.5$. In this AFM spiral or double-spiral, the orientation of the magnetic moments in one sublattice is given by $\theta = \kappa x$, and the magnetic moments on the other sublattice have the opposite directions thus keeping locally the AFM order [32].

For $J_{sd} = 5$ or smaller, the AFM order is also unstable towards an order that is staggered along the y direction and spiral along the x direction, with $\theta = \kappa x$, κ varying linearly between 0 for $\lambda/t = 0$, and $\pi/2$ for $\lambda/t \approx 0.8$. This instability of the AFM order, driven by the conduction electrons, disappears for $J \gtrapprox 0.5$.

The FM order for $J_{sd} > 5$ is also unstable towards an order that is uniform along the transversal direction and spiral along the longitudinal direction again with a pitch κ varying linearly between 0 and $\pi/2$ as in the previously mentioned staggered spiral order, which is stable for $J_{sd} < 5$. The electronically driven spiral instability of the FM layer has been already reported [43], as mentioned above, but its dependence with J_{sd}, λ/t, and W, has not been fully studied to the author's knowledge. A systematic study of these various parameters on FM spiral orders will be presented in a forthcoming study [32].

VI. CONCLUSIONS

In this work, the effects of finite strip widths on transport properties of Rashba conducting strips coupled to layers with various magnetic orders have been studied numerically at zero temperature. In the first place, it was found that for the uncoupled Rashba strip (or coupled to a nonmagnetic layer), the Drude weight slightly decreases with the Rashba SO coupling, and has a weak dependence with W. For a Rashba strip coupled to a FM layer, the Drude weight also slightly decreases with λ/t but it is strongly reduced by increasing the strip width. In both cases, the Rashba SO coupling reduces the Drude weight through processes involving solely the SO or spin-flipping currents. In addition, in the case of the FM coupling, the processes contributing to the optical conductivity are of interband origin, that is, connecting states with opposite signs of s^y. In contrast, for the uncoupled Rashba strips, these processes are completely of interband nature for the narrowest strip with $W = 2$, but the contribution from intraband transitions starts to grow with increasing W until it becomes approximately equal to the one of interband transitions, in the whole range of λ/t examined.

For the AFM coupled layer, due to the opening of gaps in the single-particle spectrum, the Drude weight has a more complex behavior. For all strip widths and Rashba SO couplings considered, its value is in general much smaller than for the other two cases studied, and it is much strongly suppressed by λ/t. This suppression is due both to processes involving spin-conserving and spin-flipping currents. For the narrowest strips, $W = 2$ and 4, D even vanishes at some finite value of λ/t. Certainly, this different behavior with respect to the other two cases, which are metallic, indicates the proximity to an insulating behavior in the AFM case.

Of course, the most relevant results for spintronic applications are those concerning the spin Hall conductivity. In this sense, the main result is that σ_{sH} in the coupled AFM system is nearly two orders of magnitude larger than the one in the coupled FM system for virtually all values of W and λ/t. It would be tempting to relate this result with the recent finding of Néel spin-orbit torques driving domain walls at velocities two orders of magnitude greater than the ones in ferromagnets [20,21], but this feature belongs to off-equilibrium regimes.

It is also important to emphasize that, for strips coupled to an AFM layer, a larger value of σ_{sH} is achieved for narrow (wide) strips at large (small) values of the Rashba SO coupling. The crossover between both regimes occurs at a value of λ/t that approximately coincides with the value at which a peak appears on the edge helical currents. Actually, the behavior of σ_{sH} with W and λ/t is quite similar to the one obtained for uncoupled Rashba strips. However, in the uncoupled case, σ_{sH} is entirely due to processes involving charge SO currents along x and spin hopping currents along y, while in the AFM

case, there are also contributions from processes involving spin hopping currents along y, although these contributions have opposite sign to the former ones, except for $\lambda/t < 0.1$.

The orientation of the magnetic moments for the AFM coupled layer [21] has also been examined. It is interesting to note that for $W = 4$, σ_{sH} is largest at small λ/t when the magnetic moments are oriented along the z direction, while for magnetic moments oriented along the x axis, which is the case studied in Ref. [17], σ_{sH} is largest at large λ/t.

Finally, in systems where the conducting-magnetic layers exchange J_{sd} is due to a Hund coupling between conducting and localized orbitals of a transition metal oxide, which may be the case of devices involving $SrTiO_3$ interfaces, the ordering of the magnetic moments is determined by the dynamics of the competing degrees of freedom. In these systems, the AFM order become unstable at small and intermediate values of λ/t with respect to a double spiral order, where both the Drude weight and σ_{sH} essentially vanish for all W.

ACKNOWLEDGMENTS

Useful discussions with C. Gazza, I. Hamad, and G. Meza, are gratefully acknowledged. The author is partially supported by the Consejo Nacional de Investigaciones Científicas y Técnicas (CONICET) of Argentina through grant PIP No. 11220120100389CO.

[1] S. A. Wolf, D. D. Awschalom, R. A. Buhrman, J. M. Daughton, S. von Molnar, M. L. Roukes, A. Y. Chtchelkanova, and D. M. Treger, Science **294**, 1488 (2001).
[2] G. A. Prinz, Science **282**, 1660 (1998).
[3] I. Zutic, J. Fabian, and S. Das Sarma, Rev. Mod. Phys. **76**, 323 (2004).
[4] D. Awschalom, Physics **2**, 50 (2009).
[5] E. I. Rashba, Sov. Phys. Solid State **2**, 1109 (1960); Yu. A. Bychkov and E. I. Rashba, JETP Lett. **39**, 78 (1984).
[6] R. Winkler, *Spin-Orbit Coupling Effects in Two-Dimensional Electron and Hole Systems* (Springer, New York, 2003).
[7] J. Sinova, S. O. Valenzuela, J. Wunderlich, C. H. Back, and T. Jungwirth, Rev. Mod. Phys. **87**, 1213 (2015).
[8] A. Hoffmann, IEEE Trans. Magn. **49**, 5172 (2013).
[9] D. Bercioux and P. Lucignano, Rep. Prog. Phys. **78**, 106001 (2015).
[10] A. Manchon and S. Zhang, Phys. Rev. B **78**, 212405 (2008).
[11] A. Manchon and S. Zhang, Phys. Rev. B **79**, 094422 (2009).
[12] X. Wang and A. Manchon, Phys. Rev. Lett. **108**, 117201 (2012).
[13] I. M. Miron, G. Gaudin, S. Auffret, B. Rodmacq, A. Schuhl, S. Pizzini, J. Vogel, and P. Gambardella, Nat. Mater. **9**, 230 (2010).
[14] D. A. Pesin and A. H. Mac Donald, Phys. Rev. B **86**, 014416 (2012).
[15] F. Freimuth, S. Blügel, and Y. Mokrousov, Phys. Rev. B **90**, 174423 (2014).
[16] A. S. Núñez, R. A. Duine, P. Haney, and A. H. MacDonald, Phys. Rev. B **73**, 214426 (2006).
[17] J. Zelezny, H. Gao, K. Vyborny, J. Zemen, J. Masek, A. Manchon, J. Wunderlich, J. Sinova, and T. Jungwirth, Phys. Rev. Lett. **113**, 157201 (2014).
[18] P. E. Roy, R. M. Otxoa, and J. Wunderlich, Phys. Rev. B **94**, 014439 (2016).
[19] P. Wadley, B. Howells, J. Zelezny, C. Andrews, V. Hills, R. P. Campion, V. Novak, F. Freimuth, Y. Mokrousov, A. W. Rushforth, K. W. Edmonds, B. L. Gallagher, and T. Jungwirth, Science **351**, 587 (2016).
[20] O. Gomonay, T. Jungwirth, and J. Sinova, Phys. Rev. Lett. **117**, 017202 (2016).
[21] J. Zelezny, H. Gao, A. Manchon, F. Freimuth, Y. Mokrousov, J. Zemen, J. Masek, J. Sinova, and T. Jungwirth, arXiv:1604.07590.
[22] Y. Kato, R. C. Myers, A. C. Gossard, and D. D. Awschalom, Science **306**, 1910 (2004).
[23] T. Jungwirth, J. Wunderlich, and K. Olejník, Nat. Mater. **11**, 382 (2012).
[24] J. A. Riera, Phys. Rev. B **88**, 045102 (2013).
[25] J. Sinova, D. Culcer, Q. Niu, N. A. Sinitsyn, T. Jungwirth, and A. H. MacDonald, Phys. Rev. Lett. **92**, 126603 (2004).
[26] E. I. Rashba, Phys. Rev. B **70**, 201309 (2004).
[27] P. L. Krotkov and S. Das Sarma, Phys. Rev. B **73**, 195307 (2006).
[28] H. Y. Hwang, Y. Iwasa, M. Kawasaki, B. Keimer, N. Nagaosa, and Y. Tokura, Nat. Mater. **11**, 103 (2012).
[29] S. Banerjee, O. Erten, and M. Randeria, Nat. Phys. **9**, 626 (2013).
[30] I. J. Hamad, C. J. Gazza, and J. A. Riera, Phys. Rev. B **93**, 205113 (2016).
[31] G. A. Meza and J. A. Riera, Phys. Rev. B **90**, 085107 (2014).
[32] G. A. Meza and J. A. Riera, in preparation (2017).
[33] N. Bovenzi, F. Finocchiaro, N. Scopigno, D. Bucheli, S. Caprara, G. Seibold, and M. Grilli, J. Supercond. Nov. Magn. **28**, 1273 (2015).
[34] S. Caprara, F. Peronaci, and M. Grilli, Phys. Rev. Lett. **109**, 196401 (2012).
[35] R. M. Fye, M. J. Martins, D. J. Scalapino, J. Wagner, and W. Hanke, Phys. Rev. B **44**, 6909 (1991).
[36] E. I. Rashba, Phys. Rev. B **68**, 241315 (2003).
[37] J. Shi, P. Zhang, D. Xiao, and Q. Niu, Phys. Rev. Lett. **96**, 076604 (2006).
[38] Z. An, F. Q. Liu, Y. Lin, and C. Liu, Sci. Rep. **2**, 388 (2012).
[39] In addition, $[H_{\text{int},y,l}, \hat{s}_l^z] = 0$, if the direction of the magnetic moments is along the z direction.
[40] S. D. Ganichev and L. E. Golub, Phys. Status Solidi B **251**, 1801 (2014).
[41] H. Li, H. Gao, L. P. Zârbo, K. Výborný, X. Wang, I. Garate, F. Doğan, A. Čejchan, J. Sinova, T. Jungwirth, and A. Manchon, Phys. Rev. B **91**, 134402 (2015).
[42] A. Qaiumzadeh and M. Titov, Phys. Rev. B **94**, 014425 (2016).
[43] K.-W. Kim, H.-W. Lee, K.-J. Lee, and M. D. Stiles, Phys. Rev. Lett. **111**, 216601 (2013).